

Electronic continua in time-resolved photoelectron spectroscopy.

I. Complementary ionization correlations

V. Blanchet,^{a)} M. Z. Zgierski, and Albert Stolow^{b)}

Steacie Institute for Molecular Sciences, National Research Council, Ottawa, Ontario, Canada K1A 0R6

(Received 14 June 2000; accepted 20 October 2000)

We examine the role of electronic continua in time-resolved photoelectron spectroscopy studies of polyatomic nonadiabatic dynamics. We have investigated the two limiting cases for such studies. We consider here the limiting case of complementary ionization correlations where the two nonadiabatically coupled excited electronic states (S_2 and S_1) correlate (in the Koopmans' picture) to different cation electronic states. We show, using an example of ultrafast internal conversion a linear polyene, that this favorable case allows for disentangling of the electronic population dynamics from the coupled vibrational dynamics. In the following paper, we investigate the unfavorable case of corresponding ionization correlations. © 2001 American Institute of Physics. [DOI: 10.1063/1.1331636]

INTRODUCTION

The excited state dynamics of polyatomic molecules is dominated by the nonadiabatic coupling of vibrational and electronic degrees of freedom. This mixing of electronic and nuclear motions induces both charge redistribution and energy flow in molecules. It is the primary step in the photochemistry of polyatomic molecules,¹ photobiological processes such as vision² and photosynthesis, and underlies many concepts in molecular electronics.³ The Born–Oppenheimer approximation (BOA) plays the pivotal role in defining the potential energy surface that allows us to represent nuclear trajectories, thus permitting a mechanistic picture of molecular dynamics. The BOA is exact provided that the nuclear kinetic energy is negligible. Breakdown of the BOA, therefore, is *uniquely* due to the motions of the atoms and occurs at the intersections or near intersections of potential energy surfaces belonging to different electronic configurations.⁴ The nonzero matrix elements of the nuclear kinetic energy operator which induce these transitions between zeroth order states are due to the so-called “promoting modes.” These radiationless transitions^{5–10} often lead to complex, broadened absorption spectra due to the high density of nuclear states and a strong variation of transition dipole with nuclear coordinate.

High resolution spectroscopy provides the most detailed insights into these processes, as in the cases of the Renner–Teller and Jahn–Teller effects¹¹ and conical intersections.¹² In some larger molecules such as pyrazine, “exact” solutions to the radiationless transition problem have been demonstrated.¹³ In general, however, it remains a challenging problem when the state density becomes very high and multi-mode vibronic couplings are involved. Especially challenging is the case of greatest interest to photochemistry—when the zeroth order excited states are directly or indirectly

coupled to a true continuum, leading to nonadiabatic photodissociation dynamics.^{14,15}

Rapid electronic dephasing leading to a strong reduction in transition dipole generally limits the spectroscopic “observation” of excited state dynamics to times within the electronic dephasing time, T_2^* . A classic example of this is the $S_2 \leftarrow S_0$ absorption spectrum of butadiene in which the very broad vibrational structure cannot be resolved.¹⁶ Double resonance, such as resonance Raman spectroscopy, which projects the excited state back onto the ground electronic state, can reveal details of the *initial* excited state dynamics^{17–19} but, importantly, only for times on the order of T_2^* . To obtain information about the molecular dynamics after T_2^* , i.e., on the “dark” state, double resonance techniques where the final state is *not* the ground electronic state will be useful.

In this paper we consider an alternative approach to these problems, through the use of time domain techniques.²⁰ The large bandwidth of a femtosecond pump pulse allows for preparation of a coherent nonstationary superposition of molecular eigenstates—a wave packet. The wave packet evolution is monitored via a coherent (femtosecond) probe pulse which projects it onto a final state as a function of time. The set of these coherent two-photon transitions contains interferences between degenerate transitions which depend on the evolving phase factors of the molecular eigenstates; in other words, the signal modulations depend on the dynamical evolution of the wave packet.

The femtosecond pump–probe technique has been successfully applied to a wide range of problems in gas phase chemical dynamics.^{20–31} The choice of the final state onto which the wave packet is projected is very important as it affects the information content and determines the experimental method (e.g., detection of photons versus particles). The particular choice of the molecular ionization continuum as a final state has been argued^{32–35} because the ground state of the ion is often well known, ionization is a universal detection scheme (no “dark” states), and multiply differential detection techniques such as photoelectron spectroscopy may

^{a)}Present address: Lab. Collisions, Agrégats, Réactivité, IRSAMC, UMR5589 du CNRS, Toulouse, France.

^{b)}Author to whom correspondence should be addressed. Electronic mail: albert.stolow@nrc.ca

be employed, increasing the information content of the measurement.

Femtosecond time-resolved photoelectron spectroscopy (TRPES: for a recent review, see Ref. 36) is beginning to be applied to a variety of problems. Its application to polyatomic nonadiabatic dynamics was studied theoretically ten years ago³⁷ and first demonstrated for the case of S_1-S_0 internal conversion in hexatriene.³⁸ TRPES has been applied to wave packet dynamics in simple systems,^{32,39-42} intramolecular vibrational energy redistribution,⁴³⁻⁴⁵ nonadiabatic intramolecular dynamics (internal conversion),⁴⁶⁻⁵² photodissociation dynamics,^{53,54} picosecond spin-orbit coupling (intersystem crossing),^{55,56} intracuster reaction dynamics,⁵⁷ excited state proton transfer dynamics,⁵⁸ and model molecular electronic switches.⁵⁹ The outgoing photoelectron may be differentially analyzed as a function of time not only with respect to kinetic energy but also angular distributions⁶⁰⁻⁶⁹ and even spin polarization.⁷⁰ Additionally, time-resolved photoelectron-photoion coincidence (PEPICO)⁵⁰ and photoelectron-photoion coincidence-imaging⁷¹ spectroscopies have been demonstrated.

We consider here the role of the electronic structure of the ionization continuum in time-resolved photoelectron spectroscopy experiments. The molecular ionization continuum contains two types of electronic structures: that due to the ion core and that due to the free electron. The electronic structure due to the ion core is simply the set of electronic states of the cation. Electronic Koopmans-type correlations upon photoionization of neutral excited state molecular orbitals may or may not, depending on the symmetries involved, allow for disentangling of electronic population dynamics from vibrational dynamics. In the present paper we consider one of the limiting cases, that of *complementary* ionization correlations, which favors the disentangling of complex vibronic dynamics. When the electronic correlations are mutually exclusive, the nonadiabatically coupled excited neutral states correlate to different ion continua provided that the coupled states are of differing symmetry (as is often the case). In this limiting case, the electronic population dynamics can be separated from the coupled vibrational wave packet dynamics even in the presence of large geometry changes upon nonadiabatic crossing or ionization. We demonstrate this possibility using the example of ultrafast internal conversion in a linear polyene.

In the second, following paper, we consider the other limiting case of electronic correlations, that of *corresponding* ionization correlations, which in general are expected to hinder the disentangling. In these cases, where the nonadiabatically coupled excited states correlate to the *same* ion continua, considerations of the geometry changes (displacements) upon nonadiabatic crossing and ionization become important. We discuss this case using examples of ultrafast internal conversion in the polyaromatic hydrocarbons phenanthrene and naphthalene.

Finally, in a forthcoming third paper, the use of the electronic structure of the free electron (the partial wave structure of the continuum) in wave packet measurements is considered from a theoretical point of view, using the general nonperturbative formalism developed by Seideman.^{62,68} The

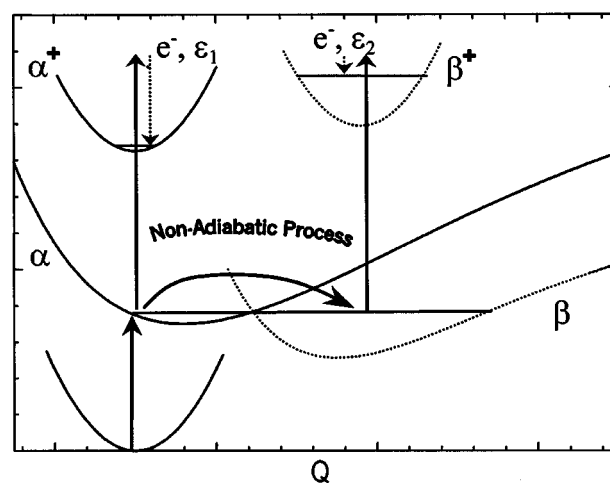


FIG. 1. A picture of polyatomic nonadiabatic dynamics. The α state prepared by the pump laser decays into the lower lying β state due to nonadiabatic coupling. Here we assume that for these two states the Koopmans-type correlations upon ionization are *complementary*: The α state preferentially ionizes into the α^+ ground state ion continuum, whereas the β state preferentially ionizes into the β^+ ion continuum, here shown as a cation excited state. This scheme should allow the disentangling of electronic from vibrational dynamics during nonadiabatic processes, as discussed in the text.

partial wave distribution, that is to say, the photoelectron angular distribution, is also generally sensitive to the electronic symmetry of the state undergoing photoionization. Thus the measurement of time-resolved photoelectron angular distributions (PADS) gives another route to the potential disentangling of complex vibronic molecular dynamics. We explore several different symmetry cases and discuss effects important in the determination of PADS.

ION ELECTRONIC CONTINUA

We consider now in more detail the role of the electronic symmetry of the final (ion) state in pump-probe photoionization experiments. Photoelectron spectroscopy is a spectroscopy of electronic configurations that remains directly sensitive to vibrational dynamics. A simplified but very useful picture is that emission of an independent outer electron occurs without simultaneous electronic reorganization of the ion core (known as the Koopmans' or frozen core approximation).^{72,73} Partial ionization probabilities (i.e., ionization into specified ion electronic states) can differ drastically with respect to the molecular orbital nature of the neutral electronic state.^{74,75} If a given electronic configuration correlates, upon removal of the outermost electron, to the electronic configuration of the ground electronic state of the cation, then the corresponding photoionization probability is much higher than if it does not. In other words, one-photon one-electron operations are more probable than one-photon two-electron operations.

In Fig. 1 we show a picture of the excited state dynamics relevant to many polyatomic systems. A zeroth order "bright" state, α , is coherently prepared with a femtosecond pump pulse. According to the Koopmans' picture, it ionizes into the α^+ continuum, the electronic state of the ion ob-

tained upon single-photon, single active electron ionization of the outermost electron. This process produces a photoelectron band ϵ_1 . In this example, we have chosen α^+ to be the ground electronic state of the ion. We now consider a nonadiabatic process which transforms the zeroth order bright state into a zeroth order “dark” state, β , as induced by promoting vibrational modes of the appropriate symmetry. By the same arguments, the β state should ionize into the β^+ ionization continuum, producing a photoelectron band ϵ_2 . Here we discuss the case of complementary correlations and assume that β^+ is an electronically excited state of the cation, as would be the case, for example, if β contained doubly excited configurations. Therefore, if we use a sufficiently energetic probe photon such that both the α^+ and β^+ continua are open channels, we would expect a switching of the electronic ionization channel from ϵ_1 to ϵ_2 during the nonadiabatic process. This picture suggests that we should be able to directly monitor *both* the changing electronically excited state symmetry (i.e., the electronic population dynamics) *and* the coupled vibrational wave packet dynamics during ultrafast nonadiabatic processes. The use of photoionization electronic correlations was considered in picosecond time scale electronic population flow during intersystem crossing.⁵⁵ On femtosecond time scales, photoelectron spectroscopy remains a vibrationally resolved technique and therefore the accompanying nuclear dynamics which promotes and tunes nonadiabatic dynamics can be observed via the detailed structure of the ϵ_1 and ϵ_2 bands. Intramolecular vibrational energy redistribution (IVR) in the α state which, by definition does not alter electronic symmetries, can be observed via the α^+ photoelectron band ϵ_1 . Similarly, IVR in the β state can be observed via the β^+ band ϵ_2 . If this picture is correct, we have in principle a method to disentangle vibrational from electronic population dynamics even though they are coupled. This could, when combined with quantum dynamical calculations, yield unprecedented views of the promoting and tuning mode dynamics as well as a direct view of the extent of and time scale for IVR on the “dark” potential energy surface. Recently, we demonstrated that such disentangling is possible via TRPES, using the example of femtosecond internal conversion in a linear polyene, *all trans* decatetraene^{47,48} and discuss these results in detail below.

LINEAR POLYENE PHOTOPHYSICS

Linear polyenes are hydrocarbon chains that have long been an area of fundamental and applied research.⁷⁶ Their nonadiabatic dynamics leads to the fundamental process of *cis-trans* photoisomerization. Polyenes form the light-harvesting antennae in vision (rhodopsin)² and light-driven transmembrane proton pumps (bacteriorhodopsin). The investigation of polyene photophysics is central to our understanding of electron delocalization and electron correlation in molecules. They have also been a test bench for quantum chemical theory due to their lowest excited state containing doubly excited configurations.⁷⁷

All trans 2,4,6,8, decatetraene (DT) provides a classic example of internal conversion in a polyene,^{76,78,79} the key photoinitiated dynamics being *cis-trans* isomerization.⁸⁰ A

great deal of the investigations on polyenes and their substituted analogs have been devoted to the ordering of excited electronic states, revealing that for simple polyenes with more than three double bonds⁸¹ the first excited state has doubly excited character, whereas the first dipole-allowed state is the second excited state.⁸² In DT, the lowest excited state is the one-photon forbidden $2^1A_g(S_1)$ state and the second excited state is the one-photon allowed $1^1B_u(S_2)$ state [the HOMO(π) \rightarrow LUMO(π^*) transition]. The $1^1B_u(S_2)$ state retains a planar structure.⁸³ The electronic origin of the S_2 state appears in the jet-cooled fluorescence excitation spectrum at $34\,784\text{ cm}^{-1}$ (4.3 eV). The electronic origin of the S_1 state in DT has been observed at $28\,963\text{ cm}^{-1}$ (3.6 eV) via two-photon fluorescence excitation.⁸³ When the energy gap between S_2 and S_1 is large, the density of S_1 vibronic levels can be very large compared to the reciprocal electronic energy spacing and the dark state forms an apparently smooth quasicontinuum. Such a situation is known as the statistical limit for the radiationless transition problem. The S_2-S_1 energy gap in DT is 5764 cm^{-1} (0.71 eV) placing this large molecule (66 modes) in this statistical limit. The statistical *versus* intermediate cases are discussed in more detail in the following paper and references therein. The 22 cm^{-1} bandwidth of the S_2 origin places a lower (Lorentzian) limit on internal conversion time scale to S_1 of around 200–300 fs.⁸⁴ There is a rapid decrease in spectral structure at $\sim 2000\text{ cm}^{-1}$ and no resolvable structure beyond 4300 cm^{-1} above the S_1 origin. The lifetime of S_1 decreases drastically beyond 3000 cm^{-1} above the origin, and is attributed to *trans-cis* isomerization.^{85–87} In comparison with octatetraene, the methyl end groups increase the state density and, via interaction between the methyl torsion and low-frequency skeletal modes of the chain, likely lead to a decrease in planarity and an increase in the internal conversion rate. (The torsional barrier is significantly reduced in S_1 relative to S_2 .) It is well known that nonplanarity leads to extremely fast internal conversion in butadiene and hexatriene.⁸⁸

In Table I we show the π molecular orbital occupancy, electronic origins (in eV), and semi-empirical weights for neutral and cation electronic states of DT. The ground states of the neutral and cation were calculated via the B3P86/6-31G* and CASSCF(7,8)/6-31G* methods. CASSCF methods were also used for the calculation of the $2^1A_g(S_1)$ and $1^1B_u(S_2)$, as well as excited cation D_1 and D_2 states. The B3P86/6-31G* method was also used to calculate some higher cation excited states. The weights were obtained from the semi-empirical QCFF/PI+CISD method in which all singly and doubly excited configurations in the π -orbital 4×4 MO space were used.^{89,90} It can be seen that the S_2 state correlates, upon removal of the highest lying electron, with the D_0 ground state of the cation, whereas the S_1 state correlates predominately with the D_1 excited state of the cation. Thus we can see that DT provides an example of the case of complementary ionization correlations. We note, as discussed in more detail below, that the geometry changes between S_2 and S_1 and between D_0 and S_1 are significant (there is bond order inversion between S_1 and S_0). This usually leads to large amplitude motion and long vibrational

TABLE I. Molecular orbital configurations, semi-empirical weights, and term energies in *all-trans* 2,4,6,8-decatetraene. The optically bright state S_2 (4.3 eV) state is singly excited, whereas the lower lying dipole-forbidden excited S_1 (3.6 eV) state results from the interaction of both singly and doubly excited configurations. The last column shows the cation electron configuration expected upon a Koopmans'-type single-photon, single active electron ionization. It can be seen that S_2 correlates with the D_0 cation ground state configuration at 7.3 eV, whereas S_1 correlates predominantly with the D_1 cation excited state configurations at 8.5 eV. It is therefore expected that the photoionization electronic channel should switch from D_0+e^- to D_1+e^- during the $S_2 \rightarrow S_1$ internal conversion. For details, see the text.

Electronic state	Energy (ev)	Molecular orbital occupancy						QCFF/PI + CISD weight	Correlated ion state
		$1a_u$	$1b_g$	$2a_u$	$2b_g$	$3a_u$	3bg		
Neutral									
$S_0, 1^1A_g$	0.0	2	2	2	2			89%	$D_0, 1^2B_g$
$S_1, 2^1A_g$	3.6	2	2	2	0	2		35%	$D_1, 1^2A_u$
		2	2	1	2	1		19%	$D_1, 1^2A_u$
$S_2, 1^1B_u$	4.3	2	2	2	1	0	1	19%	$D_0, 1^2B_g$
		2	2	2	1	1		95%	$D_0, 1^2B_g$
Cation									
$D_0, 1^2B_g$	IP=7.3	2	2	2	1			96%	
$D_1, 1^2A_u$	8.7	2	2	1	2			53%	
		2	2	2	0	1		41%	
$D_2, 2^2A_u$	9.6	2	2	1	2			38%	
		2	2	2	0	1		43%	
$D_3, 2^2B_g$	9.7	2	1	2	2			56%	
		2	2	2	0	0	1	20%	

progressions. It is of interest to see how these effects hamper the desired disentangling of electronic from vibrational dynamics.

EXPERIMENT

The molecular beam pump-probe photoelectron-photoion spectroscopy technique used in these experiments has been previously described.³⁴ Briefly, synchronized ps Nd:YAG oscillator pulses (phase-locked to a fs Ti:Sa oscillator) are regeneratively amplified at a 20 Hz repetition rate to the 100 mJ level. After frequency doubling, the high power ps 532 nm pulses are used to pump three prism dye cell amplifier chains. The first chain provides μJ level 75 fs Ti:Sa pulses at 765 nm, which are used to generate two white light continua. These are independently amplified in the other two dye chains to provide broadly tunable 60–100 fs pulses in the visible, with ~ 0.5 mJ energies after compression. Harmonic generation from these pulses gave the pump and probe pulses required for the experiments. A variable temperature pulsed molecular beam valve ($T < 200^\circ\text{C}$) was used to introduce the seeded molecular beam into the extraction region of a dual flight tube photoelectron-photoion spectrometer. As illustrated by Fig. 2, both ions and electrons could be monitored as a function of time. Isomerically pure *all-trans* 2,4,6,8 decatetraene (DT) was synthesized from the Wittig reaction between hexadienal and crotyltriphenylphosphonium bromide.⁷⁸

DT was sublimed at 30°C into 600 Torr of He carrier gas. This temperature was high enough to obtain sufficient vapor pressure (~ 0.5 Torr) yet low enough to avoid rapid polymerization of the sample. The sample was exchanged daily and there was no evidence of clusters in the beam.

The 100 fs, 2 μJ pump pulse was centered at 287 nm, the electronic origin of the S_2 state. The probe pulse wavelength was varied in order to explore the role of different ion core electronic continua on the form of the pump-probe photoelectron spectra. The two probe wavelengths used in these experiments were 235 nm (250 fs, 1 μJ) and 352 nm (100 fs, 3 μJ). Both pump and probe laser pulses were recompressed via fused silica prism pairs before entering the vacuum chamber.

The absolute $\Delta t = 0$ and laser cross correlation were determined via nonresonant 1+1 ionization of NO and 1+2 ionization of Xe. Using a $f/80$ spherical aluminum mirror to focus the pulses in the interaction region, we estimate that the pump laser intensity was $\sim 10^{11}$ W/cm², whereas the probe laser intensity was $\sim 10^{10}$ W/cm². At these intensities and frequencies, the ponderomotive broadening⁹¹ of the pho-

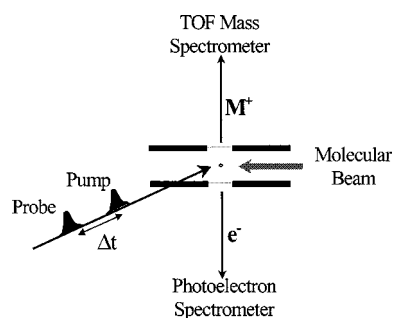


FIG. 2. A depiction of the time-resolved photoelectron spectroscopy experiment. A molecular beam is crossed by copropagating pump (excitation) and probe (ionization) fs laser pulses in the interaction region of the spectrometer. Both ions and photoelectrons may be collected as a function of the pump-probe delay time Δt .

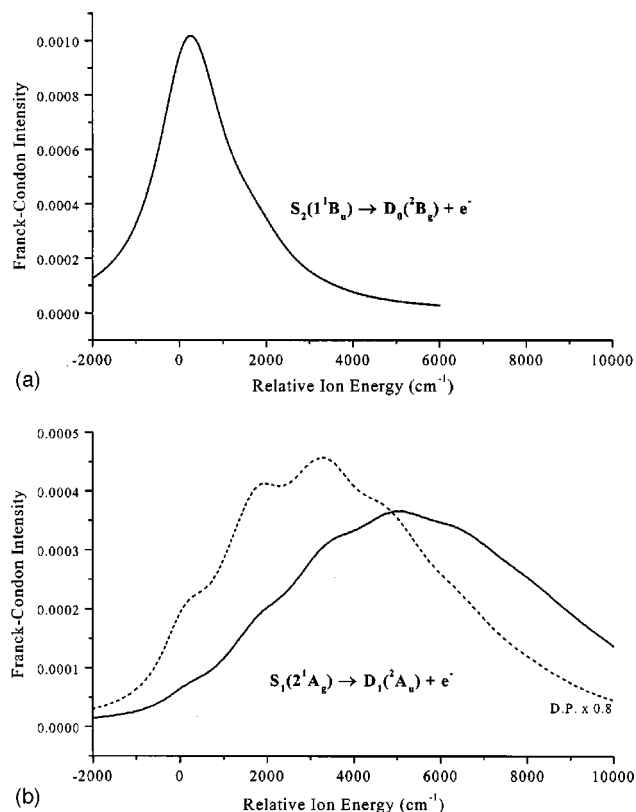


FIG. 3. (a) Calculated CASSCF-DFT Franck-Condon progression for the $S_2 \rightarrow D_0$ transitions in DT, convoluted with a 75 meV instrumental function. The structure is dominated by the 0-0 transition. (b) Calculated CASSCF-DFT Franck-Condon progression for the $S_1 \rightarrow D_1$ transitions in DT, convoluted with a 75 meV instrumental function. With scaled ($\times 0.8$) displacement parameters; the result is shown as a dashed line.

photoelectron spectra is less than the effective laser bandwidths. The photoelectron kinetic energies were calibrated by photoionizing NO via three-photon transitions at 287 nm and 352 nm or a two-photon transition at 235 nm. The MCP detector subtended an $\sim 8^\circ$ solid angle for electron collection. The pump and probe laser polarizations were each parallel to the electron time-of-flight axis for all experiments. The photoelectron spectra were averaged over 10^4 laser shots with a 200 MHz multichannel scaler and background signals due to the pump and probe laser alone were subtracted. The photoelectron spectrometer resolution was ~ 100 meV at 1 eV.

RESULTS AND DISCUSSION

Cation electronic structure

To test our idea of using the electronic structure of the ionization continuum as a template, we first need to know the electronic level spacings and symmetries for the first few excited states of the DT cation. Unfortunately, to our knowledge, there is no spectroscopic information available about the low lying electronic states of the DT cation or even the ionization potential of DT. With a combination of one-laser multiphoton photoelectron spectroscopy and *ab initio* calculation, we were able to determine these. The ionization potential was measured by two-photon nonresonant ($\lambda = 289.5$ nm) ionization from the neutral ground state to be 7.3 ± 0.05

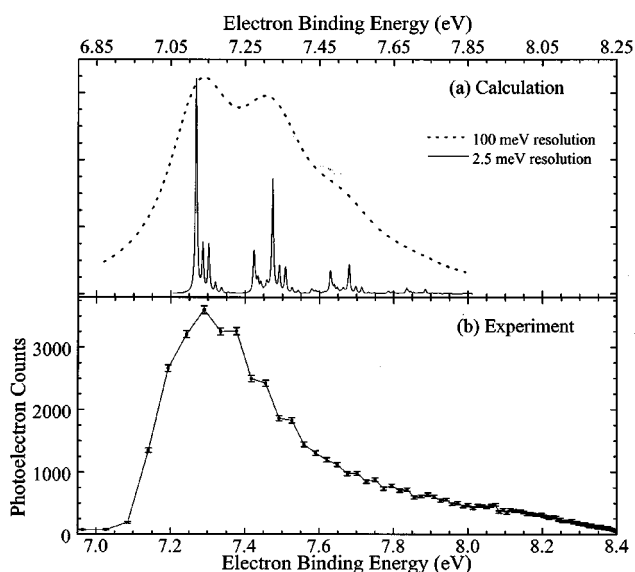


FIG. 4. One-color nonresonant two-photon ionization photoelectron spectra of DT. The fs UV pulse was centered at 289.5 nm (4.28 eV), just below the S_2 band origin. (a) Calculated CASSCF-DFT Franck-Condon progression for the $S_0 \rightarrow D_0$ transitions, at two different resolutions (2.5 meV and 100 meV). (b) The one-color, nonresonant two-photon ionization photoelectron spectrum of DT at 289.5 nm. The ionization potential was measured to be 7.3 eV.

eV, as discussed below. Two ion excited state vertical ionization potentials were determined via above threshold ionization (ATI) using three-photon transitions.

The calculated B3P86/6-31G* ionization potential (IP) is 7.12 eV. Using CASSCF geometries and force fields for S_1 and S_2 and DFT (density functional theory) geometries and force fields for D_0 and D_1 , we were able to calculate displacement parameters⁹² and Franck-Condon structure for the $S_2 \rightarrow D_0$ band, shown in Fig. 3(a), and for the $S_1 \rightarrow D_1$ band, shown in Fig. 3(b). To match the resolution at the kinetic energy expected in our experiments, the calculations are convoluted with a 75 meV instrumental width function. The relatively small geometry changes upon ionization of S_2 relative to D_0 involve four a_g modes (expansion of C=C bonds and contraction of C-C bonds). The $S_2 \rightarrow D_0$ band is strongly dominated by the 0-0 transition. By contrast, the $S_1 \rightarrow D_1$ band involves a much larger geometry change (S_1 has bond order inversion with respect to S_0). We expected that the combination of DFT and CASSCF geometries will overestimate⁹² the Franck-Condon activity of the a_g modes for the $S_1 \rightarrow D_1$ band. Therefore the result with scaled displacement parameters ($\times 0.8$) is shown by the dashed line and is compared with experiment below.

The observed *nonresonant* two-photon photoelectron spectrum is compared with calculation in Fig. 4. In Fig. 4(a) we show the Franck-Condon activity between S_0 and D_0 , showing two different resolutions (2.5 meV and 100 meV). In Fig. 4(b) we show the experimental nonresonant two-photon photoelectron kinetic energy spectrum. Both calculation and experiment are characterized by a strong origin band, supporting the calculated small geometry change between the neutral and cation ground states. Weak Franck-Condon activity is revealed in the calculated high resolution

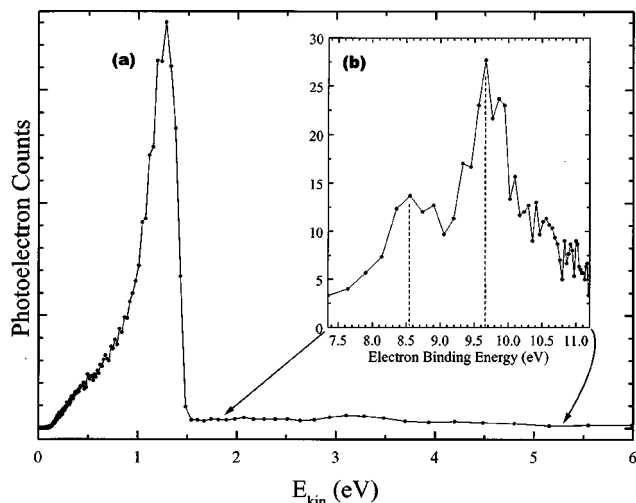


FIG. 5. One-color nonresonant multi-photon ionization photoelectron spectra of DT. The fs UV pulse was centered at 289.5 nm (4.28 eV), just below the S_2 band origin. (a) Photoelectron spectrum revealing both two-photon ionization, as in Fig. 4, and three-photon above-threshold ionization (ATI). (b) The three-photon ATI photoelectron spectrum, showing transitions to the first D_1 (at 8.55 eV) and second D_2 (at 9.67 eV) 2A_u cation electronic states, in agreement with the *ab initio* results given in Table I.

spectrum via short progressions in the a_g symmetry C=C and C-C stretches. Very weak activity connected to low-frequency CCC b_u symmetry bending vibrations is predicted. The ionization potential is estimated to be 7.12 eV. To compare with experiment, the 2.5 meV resolution spectrum was broadened to 100 meV, shown as the dashed line in Fig. 4(a). The experimental ionization potential was determined to be 7.3 eV and the overall width and shape of the spectra are in reasonable agreement. The relatively small 170 meV offset in the ionization potential, together with the similar Franck-Condon profile, gave us confidence in using the calculations to help assign the three-photon photoelectron spectrum, discussed below.

In Fig. 5(a) the experimental three-photon photoelectron spectrum is plotted as a function of kinetic energy, revealing both ionization into the ion ground state ($\epsilon_k < 1.26$ eV) and other very weak bands at higher kinetic energy ($2 < \epsilon_k < 5$ eV), signatures of ATI processes. To improve the energy resolution over this range, a retardation voltage (1 V) was applied. This spectrum is shown in Fig. 5(b), plotted as function of the electron binding energy, assuming a three-photon ionization. The two maxima observed suggest the presence of two cation excited states at 8.55 eV and 9.67 eV, respectively. The electronic symmetry expected for these two states is 2A_u since they are populated by a three-photon transition from the ground state. The calculations shown in Table II suggest a low lying 2A_u state at 1.57 eV above the ion ground state and a trio of near-degenerate states at 2.57 eV, of which one is of 2A_u symmetry. Therefore, two 2A_u excited state origins of the DT cation are predicted to lie at 8.69 eV and 9.69 eV, respectively. The two experimentally observed peaks are in good agreement. The D_1 and D_2 states of the cation consist of the same electronic configurations, the first being the symmetric and the second being the anti-symmetric combination. It should be noted, however, that

TABLE II. The vertical ionization energies predicted by CASSCF and DFT methods (see the text for details) and assignment of the peaks observed in the one-color multiphoton ionization photoelectron spectra of Figs. 4 and 5.

	D_0 1^2B_g	D_1 1^2A_u	D_2 2^2A_u	D_3 2^2B_g	D_4 3^2B_g
Theory (eV)	7.118 (I.P.)	8.69	9.62	9.71	9.91
Expt. (eV)	7.29	8.55	9.67

due to poor energy resolution, weak signals, and overlapping bands (around 9.7 eV), it is difficult to comment on the band shapes, their relative intensities, and their Franck-Condon activity. In Table II we summarize the origin bands of the ion states predicted and the assignment of the bands observed in photoelectron spectra obtained in these one-color multiphoton ionization experiments.

Pump-probe experiments at 10.6 eV total energy

In all pump-probe experiments on DT presented here, the pump pulse excited the S_2 (0,0) electronic origin at 287.5 nm. The first pump-probe experiment had a probe wavelength (235 nm) sufficient to give 2.3 eV excess energy above the ionization threshold. Therefore, dynamics occurring in the coupled S_2 - S_1 neutral states were projected onto *both* the ion ground ($D_0, 1^2B_g$) and first excited ($D_1, 1^2A_u$) electronic states. As suggested by Table I, for single-photon, single active electron emission, the S_2 state correlates with D_0 ground state producing photoelectrons with kinetic energy ϵ_1 , whereas the S_1 state correlates predominately with the D_1 excited state (at 8.55 eV), yielding photoelectron kinetic energy ϵ_2 . This is the case of complementary ionization correlations, depicted in Fig. 1. For DT, this assumption is supported by theoretical work suggesting that the ionization energies used here are low enough for independent electron approximations⁹³ and confirmed by our experimental results, below. Therefore, as the nonadiabatic coupling proceeds, we expected a switching of the photoionization electronic channel. We expect that transitions to the D_2 state (at 9.67 eV) are difficult to see due to the combination of poor Franck-Condon overlap with the highly vibrationally excited S_1 state and poor transmission of very slow electrons ($\epsilon_k < 200$ meV) through our spectrometer.

In Fig. 6 we show the measured DT parent ion signal as function of time delay between pump and probe pulses. This signal shows the rise time expected from the laser cross-correlation (Gaussian FWHM 290 ± 20 fs) and a steplike behavior at positive time delays. There appears to be a slight overall decay of the parent ion signal, with time constant 960 ± 300 fs. We note that no fragment ions were observed. The lifetime of the zeroth order S_2 state was expected to be around 0.5 ps. As might be expected, the time dependence of the total parent ion signal in this experiment appears insensitive to the electronic symmetry change induced by S_2 - S_1 internal conversion.

By contrast, as shown in Fig. 7(b), the time-resolved photoelectron kinetic energy spectrum shows a dramatically different result. Figure 7(a) shows the relevant energy level

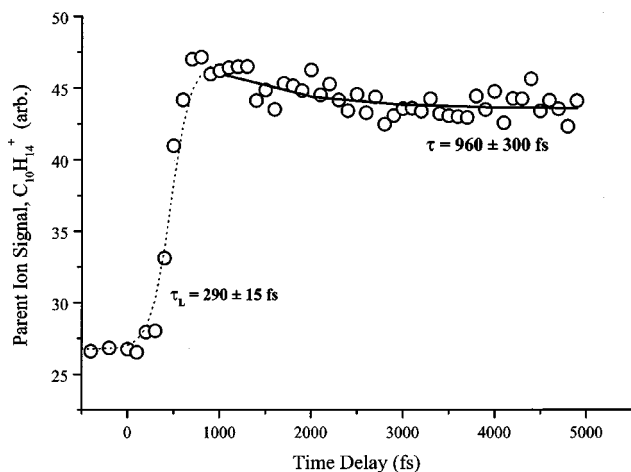


FIG. 6. Excited state dynamics at the S_2 origin of *all trans* decatetraene (DT) as measured by time-resolved photoionization mass spectrometry. The probe ionization laser (235 nm) had sufficient energy to access both the D_0 ground and D_1 first electronic states of the cation. Parent ion signals ($C_{10}H_{14}^+$) are shown as function of time delay between pump (287.5 nm) and probe pulses. No fragments were observed. The laser cross-correlation was $\tau_L = 290 \pm 20$ fs. An essentially steplike behavior is seen, showing that the ion signal in this experiment does not reveal the nonadiabatic dynamics.

scheme. We expect a shift in photoelectron spectrum from a higher energy band ($\epsilon_1 \leq 2.4$ eV) to lower energy band ($\epsilon_2 \leq 1.1$ eV) upon S_2 - S_1 internal conversion. The photoelectron spectra of Fig. 7(b) are indeed characterized by a rapid shift from a band centered at ~ 2.4 eV to a broad, structured low energy band ranging from ~ 1.6 eV to 0 eV. This rapid shift is the *direct* signature of the changing electronic configurations induced by S_2 - S_1 nonadiabatic coupling. The energetic component ($\epsilon_1 \approx 2.4$ eV) is readily assigned to the photoionization of S_2 into D_0 . The broad low energy band is assigned to photoionization of S_1 into D_1 and roughly agrees in width with the scaled Franck-Condon calculation shown in Fig. 3b. As shown in Fig. 8, integration of these two bands *directly* yields the S_2 - S_1 internal conversion times scale: 402 ± 65 fs. This clear result obtains despite the geometry changes involved.

These results demonstrate the strong selectivity of the ionization dynamics for cases of complementary ionization correlations and, importantly, show that *disentangling* of electronic population dynamics from vibrational dynamics is possible during ultrafast nonadiabatic processes.⁴⁸ If vibrational wave packet dynamics were present in S_2 (e.g., by exciting above the electronic origin) they would be revealed by the vibrational structure in the ϵ_1 band. Likewise, vibrational wave packet dynamics in S_1 is seen in the ϵ_2 band. The electronic populations dynamics accompanying the vibrational dynamics are synchronously observed via the switching from ϵ_1 to ϵ_2 .

The decaying part of the ϵ_2 band (720 ± 240 fs) and, similarly, that of the ion parent signal (Fig. 6, 960 ± 300 fs) are likely the signature of the subsequent internal conversion from S_1 to S_0 . We expect relatively poor Franck-Condon factors for “hot” ground state S_0 ionization since the probe pulse gives a maximum of 2.3 eV excess energy in the continuum, whereas the nascent “hot” S_0 ground state would

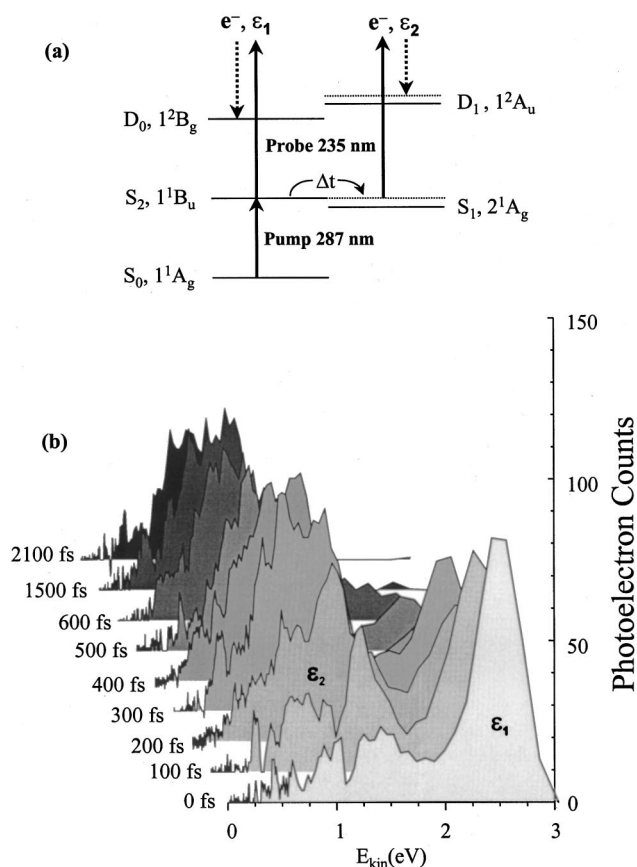


FIG. 7. Time-resolved photoelectron spectra revealing vibrational and electronic dynamics during internal conversion in *all trans* decatetraene (DT). (a) Level scheme in DT for one-photon probe ionization. The pump laser prepares the optically bright state S_2 . Due to ultrafast internal conversion, this state converts to the lower lying state S_1 with 0.7 eV of vibrational energy. The expected ionization propensity rules are shown: $S_2 \rightarrow D_0 + e^-(\epsilon_1)$ and $S_1 \rightarrow D_1 + e^-(\epsilon_2)$. (b) Femtosecond time-resolved photoelectron kinetic energy spectra of DT pumped at 287 nm and probed at 235 nm. There is a rapid (~ 400 fs) shift in the distribution: from (ϵ_1) an energetic peak at 2.5 eV due to photoionization of S_2 into the D_0 cation ground electronic state; to (ϵ_2) a broad, structured band at lower energies due to photoionization of vibrationally hot S_1 into the D_1 cation first excited electronic state. These results show a disentangling of electronic population dynamics from vibrational dynamics. The structure in the low energy band reflects the vibrational dynamics in S_1 .

contain up to 4.3 eV of vibrational energy. We note that there is a nonzero signal near 1.6 eV, seemingly in the gap between the two relevant ion states. This is due to small deviations from our simple Koopmans’ picture and corresponds to S_1 photoionization into the D_0 continuum.

A central point in this paper is that photoelectron bands in Fig. 7 contain much more information than simply the “rate constant” of the nonadiabatic process. Even with our low energy resolution, we can see some vibrational structure in the ϵ_2 photoelectron band. This, in principle, contains very detailed information about the state-to-state vibrational dynamics which promotes and tunes the electronic population transfer, as well as the ensuing IVR which the wave packet undergoes on the “dark” S_1 potential surface. We note that the S_2 state is prepared here at its vibrationless origin and therefore any vibrational dynamics observed must originate from the S_1 state. All signals decay to zero on a longer time

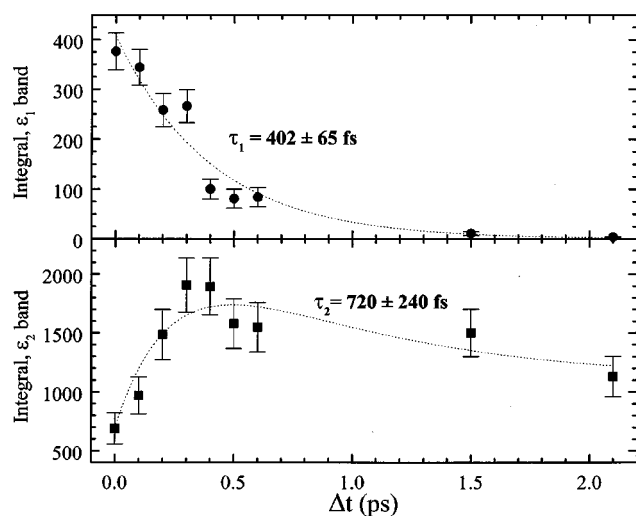


FIG. 8. Electronic population dynamics in DT at the S_2 origin. (a) The energy integrated ϵ_1 photoelectron band (1.8 eV–3.2 eV) of Fig. 7, plotted as a function of time delay, showing the decay of the S_2 state. An exponential fit directly reveals the internal conversion rate: 402 ± 65 fs. (b) The energy integrated ϵ_2 photoelectron band (<1.8 eV) of Fig. 7, plotted as a function of time delay, showing the formation and (on a longer time scale) decay of the S_1 state. This signal rises in 400 fs, due to internal conversion from S_2 and decays ~ 700 fs, presumably due to subsequent internal conversion to S_0 .

scale, presumably due to S_1 – S_0 internal conversion. Although we are not able to extract detailed information about the vibrational dynamics at the present time, a first indication that one might be able to do so eventually can be seen from Fig. 9, where we have replotted the photoelectron spectra of Fig. 7, clearly showing the changing shape of the ϵ_2 band as a function of time. We see a general shift from higher energy to lower energy electrons (i.e., higher cation vibrational energy) within this band, as a function of time. This shift is analogous to a time-dependent fluorescence red shift and suggests that we are observing an ongoing IVR process on the “dark” S_1 potential energy surface.

Many photoinduced polyatomic unimolecular reactions are based on vibrationally “hot” molecules formed via ultrafast internal conversion.⁹⁴ A fundamental approximation in unimolecular reaction rate theory is that of the assumption of statistical energy redistribution due to IVR (i.e., the complete sampling of phase space) being very fast compared with reaction.⁹⁵ Many models and interpretations are based on the supposition of fast, complete IVR. Increasingly, however, this assumption has come into question. DT has 66 internal degrees of freedom and 0.7 eV of internal energy after conversion to S_1 and is therefore expected to be in the “statistical limit.” Nevertheless, we are able to observe, via the photoelectron spectrum, some evolution in the vibrational energy distribution on the S_1 surface. We believe that our experimental method could present new views of the extent of and time scale for the onset of statisticality in an isolated, energized molecule. The detailed extraction of the vibrational wave packet dynamics associated with this internal conversion and its subsequent vibrational energy redistribution relies on modeling the multi-dimensional nonadiabatic coupling and calculating overlaps between this wave

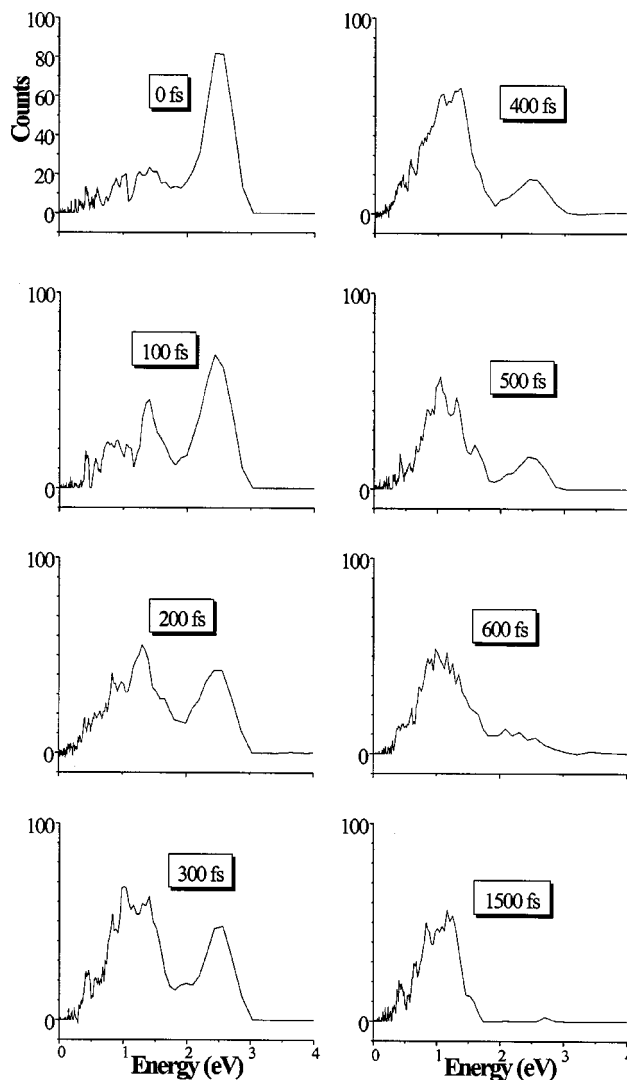


FIG. 9. Time-resolved photoelectron spectra from Fig. 7, replotted here to clearly show the changing shape of the ϵ_2 band ($\epsilon_{\text{kin}} < 1.5$ eV) as a function of time. A shift from higher energy to lower energy photoelectrons within the ϵ_2 band as a function of time is suggestive an ongoing vibrational energy redistribution process on the “dark” S_1 potential energy surface.

packet and the relevant states of the ion (work presently in progress).

Pump–probe experiments at 7.8 eV total energy

To confirm these ideas about the selectivity of the ionization continuum for specific electronic symmetries, we performed a second experiment by tuning the probe wavelength to 352 nm to yield lower excess energy in the continuum (now 0.54 eV). This is below the D_1 threshold and therefore allowing one-photon ionization into the D_0 ground ion state only. In contrast with the results of Fig. 6, we predicted that the parent ion signal would now decay in ~ 400 fs since the formed S_1 state should not correlate favorably with the D_0 continuum. In Fig. 10 we show that the time-dependent parent ion signal for 352 nm ionization is indeed well described by a decay rate of 410 ± 15 fs, confirming the above results. The fact that the parent ion signal in Fig. 10 does not decay completely to zero indicates that there remains a small tran-

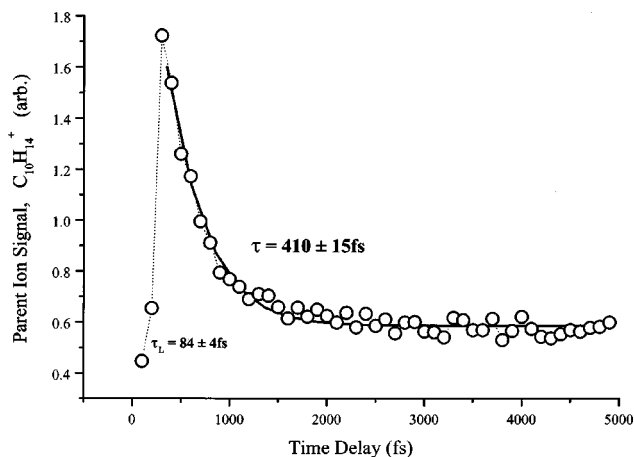


FIG. 10. Excited state dynamics at the S_2 origin of *all trans* decatetraene (DT) as measured by time-resolved photoionization mass spectrometry. In contrast with Fig. 6, the probe ionization laser (352 nm) could access only the ground electronic state of the cation. Parent ion signals ($C_{10}H_{14}^+$) are shown as function of time delay between pump (287.5 nm) and probe pulses. The signal risetime (the laser cross-correlation half-width) was $\tau_L = 84 \pm 4$ fs. The parent ion signal decays with a time constant of 410 ± 15 fs, confirming the results of Fig. 8. A behavior very different from Fig. 6 is seen, showing the crucial importance of understanding the photoionization dynamics in time-resolved ionization experiments involving nonadiabatic dynamics.

sition probability between S_1 and D_0 . The poor Franck-Condon factors associated with this transition are due to the 0.54 eV vibrational energy available in D_0 , as compared with the 0.7 eV vibrational energy in S_1 , as well as significant geometry changes between S_1 and D_0 . Comparison of the time-dependent parent ion signals at 235 nm with 352 nm probe laser wavelength clearly demonstrates that the form of the parent ion signal depends *strongly* on the specific photoionization dynamics and, in order to avoid misleading conclusions, must be analyzed for each specific case. This sensitivity of the integrated parent ion signal to the molecule-specific photoionization dynamics was previously discussed⁵⁴ in a study of the nonadiabatic dissociation dynamics of $(NO)_2$.

In contrast with the 235 nm probe experiment, the mass spectrum at 352 nm now shows fragmentation. In Fig. 11 we show the time dependence of the main fragment ion $C_9H_{11}^+$ ($m/e=119$), which corresponds to loss of a methyl end group from DT^+ . It is important to note that the D_0 , S_2 , and S_1 states are all energetically stable at these energies of pump and probe excitation and therefore the dissociation must arise from a two-photon probe transition, yielding a total energy of 11.3 eV. We note that the pump laser intensity was identical to that in the 235 nm probe experiment. However, the probe laser intensity was approximately an order of magnitude higher at 352 nm, leading us to consider the possibility of above threshold ionization (ATI). A probe laser power study supported this point, yielding a quadratic dependence for the $C_9H_{11}^+$ fragment ion and a linear dependence for the parent ion signal. This is confirmed by photoelectron spectroscopy results, discussed below. Interestingly, it can be seen that the $C_9H_{11}^+$ signal begins at almost zero near $\Delta t = 0$ and rises with a time constant of 375 ± 120 fs. This

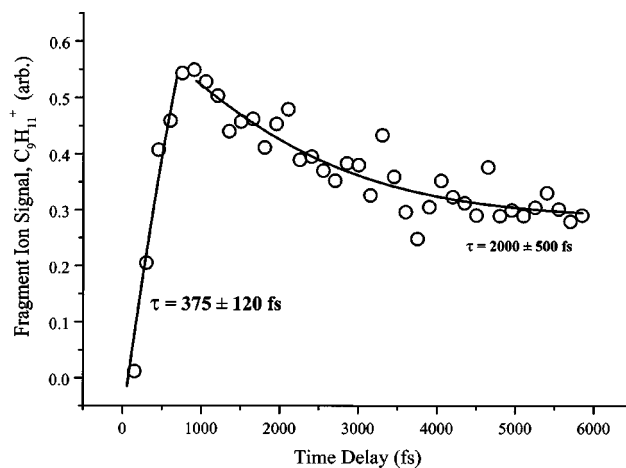


FIG. 11. A time-resolved photoionization mass spectrometry experiment showing a fragment ion signal $C_9H_{11}^+$, due to two probe photon ionization, which was determined simultaneously with the data of Fig. 10. The laser cross-correlation half-width was $\tau_L = 84 \pm 4$ fs. The fragment ion signal rises much more slowly than the parent ion signal, with a time constant of 375 ± 120 fs. This suggests that it derives from two-photon ionization of the S_1 state formed by internal conversion. On longer time scales, it appears to decay (~ 2 ps) presumably due to internal conversion of S_1 to S_0 .

strongly suggests that the fragmentation arises from two-photon ionization of the vibrationally excited S_1 state formed by the internal conversion and *not* from two-photon ionization of S_2 . This is confirmed by photoelectron spectroscopy, as discussed below.

In Fig. 12(b) we show the time-resolved photoelectron spectrum for 352 nm probe laser ionization. Initially, the spectrum is characterized by a low energy band, ϵ_1 at 0.56 eV which decays with time. As indicated in Fig. 12(a), the ϵ_1 band is due to one-photon ionization of S_2 into D_0 and corresponds exactly with the 235 nm ϵ_1 band of Fig. 7, simply shifted to lower energy by the reduction in probe photon energy. This peak is narrower due to the improved kinetic resolution at low energy. A broad energetic band, ϵ_2 , ranging from 0.6 eV to 4 eV grows with time as the ϵ_1 band decays and therefore arises from photoionization of the formed S_1 state. The ϵ_2 band must, via energy conservation, arise from two-photon probe ionization. As can be seen from Fig. 12(a), due to the symmetry of the two-photon dipole operator, the ion continua accessed via two-photon ionization may also include D_0 , D_3 , and D_4 . This explains the broad range and high kinetic energy of the photoelectrons in the ϵ_2 band. Integration of the ϵ_1 band, shown in Fig. 13(a), provides yet another independent confirmation of the S_2 - S_1 internal conversion time scale, 377 ± 47 fs, fully in agreement with the previous results. The decaying part of the ϵ_2 component integration (783 ± 109 fs), Fig. 13(b), as in Figs. 6 and 7, is likely the signature of the subsequent internal conversion between the S_1 and S_0 states.

It is interesting to consider why, at invariant probe laser intensity, the photoionization process switches from single-photon ionization of S_2 to two-photon ionization of S_1 . We note that in the both cases, the first photon is already above the ionization potential and therefore the S_1 ionization is due to absorption of a second photon in the ionization continuum (ATI). This can be rationalized by a consideration of the

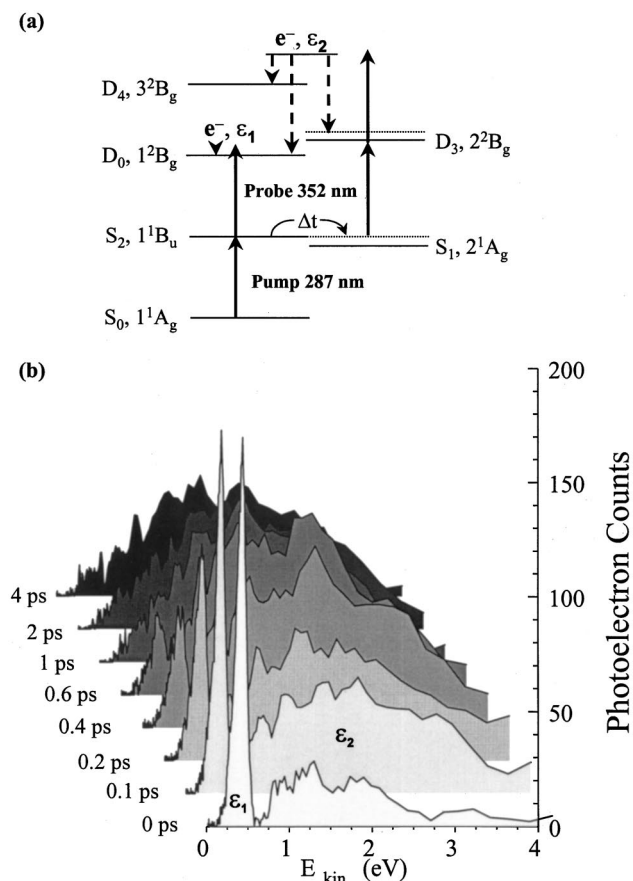


FIG. 12. Time-resolved vibrational and electronic dynamics during internal conversion for *all trans* decatetraene (DT) via two-photon ionization. (a) Level scheme in DT for one- and two-photon probe ionization. The pump laser is identical to that in Fig. 7 and prepares the same S_2 state wave packet. The expected ionization propensity rules are: $S_2 \rightarrow D_0 + e^- (\epsilon_1)$ for one-photon ($u \leftrightarrow g$, as in Fig. 7) ionization and $S_1 \rightarrow D_0, D_3, D_4 + e^- (\epsilon_2)$ for two-photon ($g \leftrightarrow g$) ionization. (b) Femtosecond time-resolved photoelectron kinetic energy spectra of DT pumped at 287 nm and probed at 352 nm, using both one- and two-photon probes. At 352 nm, the D_1 ion state is not energetically accessible from the S_1 state via a single-photon transition. Confirming the results of Fig. 7, there is a rapid shift (≈ 400 fs) in the distribution: from (ϵ_1) a peak at 0.4 eV due to one-photon ionization of S_2 into the D_0 cation ground electronic state; to (ϵ_2) a broad, structured band at higher energies (1–3.5 eV) due to two-photon ionization of the vibrationally hot S_1 into the D_0 cation ground and excited electronic states. The photoionization channel switches from a one-photon to a two-photon process during the internal conversion indicating again that the electronic structure of the ionization continuum is selective of the evolving electronic symmetry in the neutral state.

relative rates of two competing processes: second photon absorption *versus* autoionization. For the case of S_2 , the photoionization correlation is with D_0 and therefore the ionization is direct. In other words, the “autoionization” is extremely rapid and second photon absorption cannot compete. For the case of S_1 , the photoionization correlation is with D_1 . The D_1 state, however, is energetically inaccessible and therefore the transition is most likely into Rydberg series converging on the D_1 threshold. For these to emit an electron into the open D_0 continuum channel, there must be an electronic rearrangement, for which there is a finite autoionization rate. In this case, the absorption of a second photon competes effectively with autoionization. These two-photon experiments

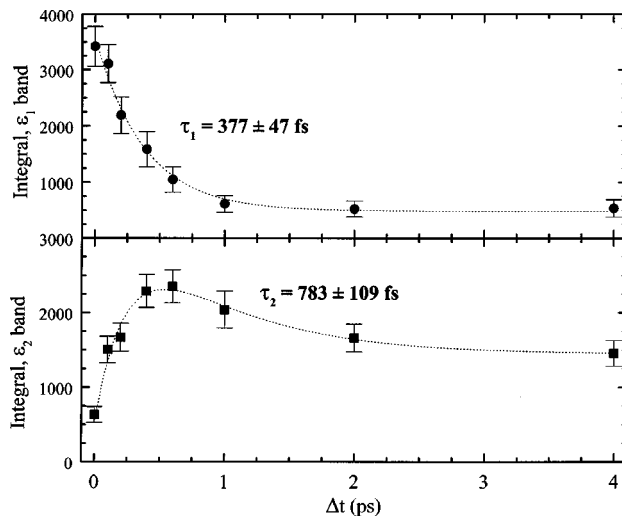


FIG. 13. Electronic population dynamics in DT at the S_2 origin via two-photon ionization. (a) The energy integrated ϵ_1 photoelectron band (< 0.56 eV) of Fig. 12, plotted as a function of time delay, showing the decay of the S_2 state. An exponential fit directly reveals the internal conversion rate: 377 ± 47 fs, confirming the previous results. (b) The energy integrated ϵ_2 photoelectron band (0.56 eV–4 eV) of Fig. 12, plotted as a function of time delay, showing the formation and (on a longer time scale) decay of the S_1 state. This signal rises in 400 fs, due to internal conversion from S_2 and again decays ~ 700 fs, confirming the previous results.

not only confirm the one-photon results, but also demonstrate the symmetry selectivity of the photoionization process itself.

CONCLUSION

Nonadiabatic processes, ubiquitous in excited state polyatomic dynamics, lead to complex wave packet evolution and strongly varying transition dipole moments due to the mixing of electronic and vibrational degrees of freedom. An important goal of our laboratory is to try to use femtosecond wavepacket methods to *disentangle* these coupled degrees of freedom in order to recover a picture of the evolution of the zeroth order Born–Oppenheimer states. We considered in detail the nature of the final state in polyatomic wave packet dynamics experiments using photoionization detection. We have argued that the molecular ionization continuum is a very interesting final state for the study of nonadiabatic polyatomic wavepackets. The vibrational aspects of the wave packet dynamics can be observed via the vibrational structure of the ionization continuum (i.e., vibrational states of the cation). The electronic structure of the continuum (i.e., the set of electronic states of the cation and the free electron partial wave structure) is sensitive to the electronic population dynamics (based on electronic propensity rules and symmetry properties of the free electron partial waves). We investigated the role of electronic continua (the cation electronic states) in femtosecond time-resolved photoelectron spectroscopy measurements and considered two limiting cases of Koopmans’-type photoionization correlations. The first case, complementary ionization correlations, discussed in this paper, is one in which the coupled states (e.g., S_2 and S_1) correlate to *different* cation electronic states. We suggested that this favorable situation can allow for a simulta-

neous monitoring of both the electronic population dynamics and the coupled vibrational wave packet dynamics.⁴⁸ The second limiting case, corresponding ionization correlations, discussed in the following paper, is one in which the coupled states (e.g., S_2 and S_1) correlate to the *same* cation electronic states.

We studied ultrafast S_2-S_1 internal conversion dynamics in *all trans* 2,4,6,8-decatetraene as an example of complementary ionization correlations. The S_2 state is singly excited and correlates with the D_0 ground state of the cation. The S_1 state, by contrast, contains doubly excited configurations and correlates preferentially with the D_1 first excited state of the cation. By pumping the molecule to the S_2 origin and then probing with a photon sufficiently energetic so as to include both the D_1 and D_0 cation states, we obtained time-resolved photoelectron spectra which revealed the change in electronic symmetry implicit in internal conversion, allowing a *direct* determination of the internal conversion time scale—400 fs. Furthermore, these spectra allowed observation of vibrational wave packet dynamics on the “dark” S_1 potential energy surface.

We confirmed these results with an independent experiment using two-photon probe laser ionization, where the first probe photon was above the D_0 ionization threshold but below the D_1 state. Again, the same picture emerges and a direct measurement of the internal conversion time obtains. We also demonstrated that although the time-resolved integrated parent ion signals in pump-probe studies of nonadiabatic dynamics may have very different forms (depending on the specifics of the photoionization dynamics), they can be readily interpreted in terms of their associated photoelectron spectra. The measurement of integrated parent ion signals alone may be potentially misleading for cases of excited state polyatomic nonadiabatic dynamics.

In the following paper, we consider the unfavorable case of corresponding ionization correlations in which we expect the disentangling of electronic from vibrational dynamics to be more challenging. In these cases, geometry changes (displacements) become an important aspect of the problem. It is also interesting to study the other component of the molecular ionization continuum, the free electron. As photoelectron angular distributions (PADS) are directly sensitive to changes in excited state electronic symmetry, experiments are presently underway both in our laboratory and elsewhere to investigate this possibility.

We hope that the time-resolved photoelectron spectroscopy method will prove useful in many situations where there are significant charge rearrangements during the excited state dynamics. In our current experimental work, we are applying time-resolved photoelectron spectroscopy to excited state proton transfer, yielding both time scales and the energy dependencies of the intramolecular processes.⁹⁶ In the area of molecular electronics, azobenzene serves as the model of an ultrafast molecular switch. We have studied the nonadiabatic intramolecular dynamics of azobenzene, determining time scales and shedding new light on the complex primary photophysical processes.⁹⁷ Of photochemical interest, the excited states of aldehydes and ketones, by contrast with polyenes studied here, can have important carbonyl

$\pi-\pi^*/n-\pi^*$ interactions. We have examined the nonadiabatic dynamics in a series of dieneones,⁹⁸ showing the importance of inductive effects on the competition between internal conversion and intersystem crossing. In the future, we plan to investigate excited state electron transfer dynamics using time-resolved photoelectron spectroscopy, with the hope of directly observing the coherent vibrational dynamics associated with the charge transfer.⁹⁹ Together with the work of many other laboratories, we are optimistic that a detailed new view of the complex nonadiabatic processes that underpin our understanding of photochemistry, material photochemicals, and molecular electronics will emerge.

ACKNOWLEDGMENTS

We thank P. Arya and M. Barnes of the Steacie Institute Chemical Biology Program for the synthesis of *all-trans* 2,4,6,8 decatetraene. We thank T. Seideman, W. Domcke, W. J. Buma, B. S. Hudson, M. Schmitt, J. P. Shaffer, T. Schultz, and J. G. Underwood for helpful discussions.

- ¹J. Michl and V. Bonacic-Koutecky, *Electronic Aspects of Organic Photochemistry* (Wiley, New York, 1990).
- ²R. W. Schoenlein, L. A. Peteanu, R. A. Mathies, and C. V. Shank, *Science* **254**, 412 (1991).
- ³J. Jortner and M. A. Ratner, *Molecular Electronics* (IUPAC, Blackwell Oxford, 1997).
- ⁴G. Herzberg and H. C. Longuet-Higgins, *Faraday Discuss.* **35**, 77 (1963).
- ⁵W. Siebrand, *J. Chem. Phys.* **47**, 2411 (1967).
- ⁶M. Bixon and J. Jortner, *J. Phys. Chem.* **48**, 715 (1968).
- ⁷J. Jortner, S. A. Rice, and R. M. Hochstrasser, *Adv. Photochem.* **7**, 149 (1969).
- ⁸B. R. Henry and W. Siebrand, *Radiationless Transitions in Organic Molecular Photophysics*, Vol. 1, edited by J. B. Birks (Wiley, London, 1973).
- ⁹K. F. Freed, in *Radiationless Processes in Molecules and Condensed Phases* edited by F. K. Fong (Springer, Berlin, 1976), p. 23.
- ¹⁰G. Stock and W. Domcke, *Adv. Chem. Phys.* **100**, 1 (1997).
- ¹¹G. Herzberg, *Molecular Spectra and Molecular Structure*, Vol. 3 (Van Nostrand, 1945, New York).
- ¹²D. R. Yarkony, *Acc. Chem. Res.* **31**, 511 (1998).
- ¹³J. Kommandeur, W. A. Majewski, W. L. Meerts, and D. W. Pratt, *Annu. Rev. Phys. Chem.* **38**, 433 (1987).
- ¹⁴R. Schinke, *Photodissociation Dynamics* (Cambridge University Press, Cambridge, 1993).
- ¹⁵L. J. Butler, *Annu. Rev. Phys. Chem.* **49**, 125 (1998).
- ¹⁶G. Orlandi, F. Zerbetto, and M. Z. Zgierski, *Chem. Rev.* **91**, 867 (1991).
- ¹⁷W. Siebrand and M. Z. Zgierski, *J. Chem. Phys.* **71**, 3561 (1979).
- ¹⁸R. J. Sension, R. J. Boudryushi, B. S. Hudson, F. Zerbetto, and M. Z. Zgierski, *J. Chem. Phys.* **96**, 2617 (1992).
- ¹⁹M. K. Lawless, S. D. Wickam, and R. A. Mathies, *Acc. Chem. Res.* **28**, 493 (1995).
- ²⁰A. H. Zewail, *Femtochemistry: Ultrafast Dynamics of the Chemical Bond* (World Scientific, Singapore, 1994).
- ²¹T. Baumert, B. Bühler, M. Grosser, R. Thalweiser, V. Weiss, E. Wiedenmann, and G. Gerber, *J. Phys. Chem.* **95**, 8103 (1991).
- ²²J. C. Owruksy and A. P. Baronavski, *J. Chem. Phys.* **108**, 6652 (1999); *ibid.* **110**, 11206 (1999).
- ²³S. A. Trushin, W. Fuss, T. Schikarski, W. E. Schmid, and K. L. Kompa, *J. Chem. Phys.* **106**, 9386 (1997).
- ²⁴H. Schwoerer, R. Pausch, M. Heid, V. Engel, and W. Kiefer, *J. Chem. Phys.* **107**, 9749 (1997).
- ²⁵R. Lopez-Martens, T. W. Schmidt, and G. Roberts, *J. Chem. Phys.* **111**, 7183 (1999).
- ²⁶T. Shibata, H. Li, H. Katayanagi, and T. Suzuki, *J. Phys. Chem. A* **102**, 3643 (1998).
- ²⁷H. Ruppe, S. Rutz, E. Schreiber, and L. Woste, *Chem. Phys. Lett.* **257**, 356 (1996); **257**, 365 (1996).
- ²⁸V. Blanchet, M. A. Bouchene, G. Cabrol, and B. Girard, *Chem. Phys. Lett.* **233**, 491 (1995).

- ²⁹ S. I. Ionov, G. A. Brucker, C. Jaques, L. Valachovic, and C. Wittig, *J. Chem. Phys.* **99**, 6553 (1993).
- ³⁰ V. Vorsa, P. J. Campagnola, S. Nandi, M. Larsson, and W. C. Lineberger, *J. Chem. Phys.* **105**, 2298 (1996).
- ³¹ U. Marvet and M. Dantus, *Chem. Phys. Lett.* **256**, 57 (1996).
- ³² I. Fischer, D. M. Villeneuve, M. J. J. Vrakking, and A. Stolow, *J. Chem. Phys.* **102**, 5566 (1995).
- ³³ I. Fischer, D. M. Villeneuve, M. J. J. Vrakking, and A. Stolow, in *Femtochemistry: The Lausanne Conference*, edited by M. Chergui (World Scientific, Singapore, 1996), p. 43.
- ³⁴ I. Fischer, M. J. J. Vrakking, D. M. Villeneuve, and A. Stolow, *Chem. Phys.* **207**, 331 (1996).
- ³⁵ I. Fischer, D. M. Villeneuve, M. J. J. Vrakking, and A. Stolow, in *Ultrafast Phenomena X*, edited by P. F. Barbara, J. G. Fujimoto, W. H. Knox and W. Zinth (Springer, Berlin, 1996), p. 187.
- ³⁶ C. C. Hayden and A. Stolow, in *Adv. Series in Physical Chemistry Vol. 10: Photoionization and Photodetachment*, edited by C. Y. Ng (World Scientific, Singapore, 2000).
- ³⁷ M. Seel and W. Domcke, *J. Chem. Phys.* **95**, 7806 (1991).
- ³⁸ D. R. Cyr and C. C. Hayden, *J. Chem. Phys.* **104**, 771 (1996).
- ³⁹ V. Engel, *Chem. Phys. Lett.* **178**, 130 (1991); Ch. Meier and V. Engel, *ibid.* **212**, 691 (1993); *J. Chem. Phys.* **101**, 2673 (1994); *Phys. Rev. Lett.* **73**, 3207 (1994).
- ⁴⁰ T. Baumert, R. Thalweiser, and G. Gerber, *Chem. Phys. Lett.* **209**, 29 (1993).
- ⁴¹ A. Assion *et al.*, *Phys. Rev. A* **54**, R4605 (1996).
- ⁴² B. J. Greenblatt, M. T. Zanni, and D. M. Neumark, *Chem. Phys. Lett.* **258**, 523 (1996).
- ⁴³ J. M. Smith, C. Lakshminarayan, and J. L. Knee, *J. Chem. Phys.* **93**, 4475 (1990).
- ⁴⁴ X. Zhang, J. M. Smith, and J. L. Knee, *J. Chem. Phys.* **100**, 2429 (1994).
- ⁴⁵ C. Lakshminarayan and J. L. Knee, *J. Phys. Chem.* **99**, 1768 (1995).
- ⁴⁶ W. Radloff, V. Stert, Th. Freudenberg, I. V. Hertel, C. Jouvot, C. Dedonder-Lardeux, and D. Solgadi, *Chem. Phys. Lett.* **281**, 20 (1997).
- ⁴⁷ V. Blanchet and A. Stolow, in *Ultrafast Phenomena XI*, edited by T. Elsaesser, J. G. Fujimoto, D. A. Wiersma, and W. Zinth (Springer, Berlin, 1998), p. 456.
- ⁴⁸ V. Blanchet, M. Z. Zgierski, T. Seideman, and A. Stolow, *Nature (London)* **401**, 52 (1999).
- ⁴⁹ C. P. Schick, S. D. Carpenter, and P. M. Weber, *J. Phys. Chem. A* **103**, 10470 (1999).
- ⁵⁰ V. Sert, W. Radloff, C. P. Schultz, and I. V. Hertel, *Eur. Phys. J. D* **5**, 97 (1999).
- ⁵¹ M. Schmitt, J. J. Larsen, S. Lochbrunner, J. P. Shaffer, M. Z. Zgierski, and A. Stolow, *J. Chem. Phys.* **1206–1213**, (2000), following paper.
- ⁵² J. P. Shaffer, T. Schultz, M. Schmitt, M. Zgierski, and A. Stolow (unpublished).
- ⁵³ M. R. Dobber, W. J. Buma, and C. A. de Lange, *J. Phys. Chem.* **99**, 1671 (1995).
- ⁵⁴ V. Blanchet and A. Stolow, *J. Chem. Phys.* **108**, 4371 (1998).
- ⁵⁵ B. Kim, C. P. Schick, and P. M. Weber, *J. Chem. Phys.* **103**, 6903 (1995).
- ⁵⁶ T. Suzuki, L. Wang, and H. Kohguchi, *J. Chem. Phys.* **111**, 4859 (1999).
- ⁵⁷ B. J. Greenblatt, M. T. Zanni, and D. M. Neumark, *Science* **276**, 1675 (1997).
- ⁵⁸ S. Lochbrunner, J. P. Shaffer, M. Schmitt, T. Schultz, M. Zgierski, and A. Stolow (unpublished).
- ⁵⁹ T. Schultz, J. P. Shaffer, M. Schmitt, M. Zgierski, and A. Stolow (unpublished).
- ⁶⁰ K. L. Reid, *Chem. Phys. Lett.* **215**, 25 (1993).
- ⁶¹ K. L. Reid, S. P. Duxon, and M. Towrie, *Chem. Phys. Lett.* **228**, 351 (1994).
- ⁶² T. Seideman, *J. Chem. Phys.* **107**, 7859 (1997).
- ⁶³ S. C. Althorpe and T. Seideman, *J. Chem. Phys.* **110**, 147 (1999).
- ⁶⁴ K. L. Reid, T. A. Field, M. Towrie, and P. Matousek, *J. Chem. Phys.* **111**, 1438 (1999).
- ⁶⁵ T. Suzuki, L. Wang, and H. Kohguchi, *J. Chem. Phys.* **111**, 4859 (1999).
- ⁶⁶ Y. Arasaki, K. Takatsuka, K. Wang, and V. McKoy, *Chem. Phys. Lett.* **302**, 363 (1999).
- ⁶⁷ S. C. Althorpe and T. Seideman, *J. Chem. Phys.* (submitted).
- ⁶⁸ T. Seideman, *J. Chem. Phys.* (submitted).
- ⁶⁹ T. Seideman and S. C. Althorpe, *J. Electron Spectrosc. Relat. Phenom.* (submitted).
- ⁷⁰ M. Aeschlimann, M. Bauer, S. Pawlik, W. Weber, R. Burgermeister, D. Oberli, and H. C. Siegmann, *Phys. Rev. Lett.* **79**, 5158 (1997).
- ⁷¹ J. A. Davies, J. E. LeClaire, R. E. Continetti, and C. C. Hayden, *J. Chem. Phys.* **111**, 1 (1999).
- ⁷² J. H. D. Eland, *Photoelectron Spectroscopy* (Butterworths, London, 1984).
- ⁷³ J. Berkowitz, *Photoabsorption, Photoionization, and Photoelectron Spectroscopy* (Academic, New York, 1979).
- ⁷⁴ C. A. de Lange, in *High Resolution Laser Photoionization & Photoelectron Studies*, edited by I. Powis, T. Baer and C. Y. Ng (Wiley, New York, 1995), p. 195.
- ⁷⁵ S. T. Pratt, P. M. Dehmer, and J. L. Dehmer, *J. Chem. Phys.* **81**, 3444 (1984).
- ⁷⁶ B. S. Hudson, B. E. Kohler, and K. Schulten, *Linear Polyene Electronic Structure and Potential Surfaces. Excited States 6* edited by E. C. Lim (Academic, New York, 1982).
- ⁷⁷ G. Orlandi, F. Zerbetto, and M. Z. Zgierski, *Chem. Rev.* **91**, 867 (1991).
- ⁷⁸ H. Petek, A. J. Bell, K. Yoshihara, and R. L. Christensen, *J. Chem. Phys.* **95**, 4739 (1991).
- ⁷⁹ F. Buda, H. J. M. de Groot, and A. Bifone, *Phys. Rev. Lett.* **77**, 4474 (1996).
- ⁸⁰ M. F. Granville, G. R. Holtom, and B. E. Kohler, *J. Chem. Phys.* **72**, 4671 (1980); H. Petek, A. Bell, Y. S. Choi, K. Yoshihara, B. A. Tounge, and R. L. Christensen, *ibid.* **98**, 3777 (1993).
- ⁸¹ W. J. Buma, B. E. Kohler, and K. Song, *J. Chem. Phys.* **94**, 6367 (1991).
- ⁸² J. R. Andrews and B. S. Hudson, *Chem. Phys. Lett.* **57**, 600 (1978).
- ⁸³ H. Petek, A. J. Bell, Y. S. Choi, K. Yoshihara, B. A. Tounge, and R. L. Christensen, *J. Chem. Phys.* **102**, 4726 (1995).
- ⁸⁴ W. G. Bouwman, A. C. Jones, D. Phillips, P. Thibodeau, C. Friel, and R. L. Christensen, *J. Chem. Phys.* **94**, 7429 (1990).
- ⁸⁵ W. J. Buma, B. E. Kohler, and T. A. Shaler, *J. Chem. Phys.* **96**, 399 (1992).
- ⁸⁶ S. Choi, T-S Kim, H. Petek, K. Yoshihara, and R. L. Christensen, *J. Chem. Phys.* **100**, 9269 (1994).
- ⁸⁷ W. J. Buma and F. Zerbetto, *J. Phys. Chem. A* **103**, 2220 (1999).
- ⁸⁸ F. Zerbetto and M. Z. Zgierski, *J. Chem. Phys.* **98**, 4822 (1993); **93**, 1235 (1990).
- ⁸⁹ A. Warshel and M. Karplus, *J. Am. Chem. Soc.* **94**, 5612 (1972).
- ⁹⁰ F. Zerbetto, M. Z. Zgierski, F. Negri, and G. Orlandi, *J. Chem. Phys.* **89**, 3681 (1988).
- ⁹¹ A. Zavriyev, I. Fischer, D. M. Villeneuve, and A. Stolow, *Chem. Phys. Lett.* **234**, 281 (1995).
- ⁹² See F. Negri and M. Z. Zgierski, *J. Chem. Phys.* **107**, 4827 (1997).
- ⁹³ G. Fronzoni, P. Decleva, A. Lisini, and G. Alti, *J. Electron Spectrosc. Relat. Phenom.* **69**, 207 (1994).
- ⁹⁴ For example, N. Nakashima and K. Yoshihara, *J. Phys. Chem.* **93**, 7763 (1989).
- ⁹⁵ W. Forst, *Theory of Unimolecular Reactions* (Academic, New York, 1973).
- ⁹⁶ S. Lochbrunner, T. Schultz, M. Schmitt, J. P. Shaffer, M. Z. Zgierski, and A. Stolow, *J. Chem. Phys.* (submitted).
- ⁹⁷ T. Schultz, A. Stolow *et al.* (unpublished).
- ⁹⁸ J. P. Shaffer, A. Stolow *et al.* (unpublished).
- ⁹⁹ M. Bixon and J. Jortner, *J. Chem. Phys.* **107**, 1470 (1997).